Available online at www.sciencedirect.com
SCIENCE DIRECT®
International Journal of Mass Spectrometry 228 (2003) 759–777
International Journal of Mass Spectrometry
www.elsevier.com/locate/ijms

The remarkable decarbonylation of $CH_3O–P{=}O^{\bullet+}$ and its distonic isomer $CH_2O–P–OH^{\bullet+}$: an experimental and CBS-QB3 computational study

Lisa N. Heydorn[a], Peter C. Burgers[b], Paul J.A. Ruttink[c], Johan K. Terlouw[a,*]

[a] *Department of Chemistry, McMaster University, Hamilton, Ont., Canada L8S 4M1*
[b] *Hercules European Research Center BV, Nijverheidsweg 60, 3771 ME, Barneveld, The Netherlands*
[c] *Theoretical Chemistry Group, Department of Chemistry, University of Utrecht, 3584 CH, Utrecht, The Netherlands*

Received 2 December 2002; accepted 31 March 2003

Dedicated to Professor Helmut Schwarz on the occasion of his 60th birthday.

Abstract

The dissociation chemistry of the title ions was investigated using tandem mass spectrometry-based experiments in conjunction with isotopic labeling and computational quantum chemistry.

Upon collisional activation, ions $CH_3O–P{=}O^{\bullet+}$ (**1a**) and $CH_2O–P–OH^{\bullet+}$ (**1b**) readily lose $CH_2{=}O$. This reaction is completely suppressed in the low-energy (metastable) ions, which instead abundantly lose CO. The product ion generated in this decarbonylation reaction is the ylide ion $H–P–OH_2^{\bullet+}$, rather than its more stable isomer $H_2P–OH^{\bullet+}$. Remarkably, the oxygen atoms become equivalent in this reaction: ions $CH_3{}^{18}O–P{=}O^{\bullet+}$ and $CH_2O–P–{}^{18}OH^{\bullet+}$ lose $C^{18}O$ and $C^{16}O$ in a 1:1 ratio. The experiments further show that the dissociating ions have a fairly large internal energy content: up to 40 kcal/mol for the distonic ion **1b**, which, along with the "enol" ion $CH_2{=}P(OH){=}O^{\bullet+}$, represents the global minimum of the $CH_3O_2P^{\bullet+}$ potential energy surface.

The mechanism of this intriguing decarbonylation was studied, using the CBS-QB3 model chemistry to probe the structure and energetics of potential intermediates and their interconversion barriers. It appears that metastable ions **1a** and **1b** have sufficient internal energy to communicate with a great many isomers. Of these, the cyclic ion $P[–OCH_2O(H)–]^{\bullet+}$ and ion $[CH_2O–H{\bullet\bullet\bullet}O{=}P]^{\bullet+}$, a hydrogen-bridged radical cation (HBRC), play a key role in the oxygen equilibration. The HBRC's $[HO–P{\bullet\bullet\bullet}H–C(H){=}O]^{\bullet+}$ and $[H–P–O(H)–H{\bullet\bullet\bullet}C{\equiv}O]^{\bullet+}$ are key intermediates in the actual mechanism for the decarbonylation. The latter ion may lose CO to produce $H–P–OH_2^{\bullet+}$ or else isomerize into the ion–dipole complex $[H_2O{\bullet\bullet\bullet}P(H){=}C{=}O]^{\bullet+}$, whose dissociation into $H_2O + H–P{=}C{=}O^{\bullet+}$ accounts for the observed minor loss of water.

Keywords: Decarbonylation; CBS-QB3 model chemistry; Hydrogen-bridged radical cations; Proton-transport catalysis; Enthalpy of formation; CH_3PO_2 isomers

1. Introduction

In the context of our studies of molecule-assisted tautomerization reactions of radical cations in ion–molecule encounter complexes [1], we recently studied

* Corresponding author. Tel.: +905-525-9140x27111; fax: +905-522-2509.
E-mail address: terlouwj@mcmaster.ca (J.K. Terlouw).

1387-3806/$ – see front matter © 2003 Elsevier B.V. All rights reserved.
doi:10.1016/S1387-3806(03)00237-9

the intriguing gas-phase ion chemistry of the dimethyl phosphonate radical cation, $(CH_3O)_2P(H)=O^{\bullet+}$, using a variety of mass spectrometry based techniques [2]. The interpretation of the experimental results relied heavily on energetic information which, given the dearth of reliable experimental enthalpy values for PO-containing ions and neutrals, was obtained from computational chemistry. From a brief validation study [2], it appears that the CBS-QB3 model chemistry [3] accurately reproduces heats of formation of species comprised of a second row element (P or S) bonded to a highly electronegative element (O). For the $(CH_3O)_2P(H)=O^{\bullet+}$ system of ions, it was further argued that a conservative estimate for the uncertainty in computed transition states/reaction barrier heights is ±4 kcal/mol [2].

This combination of theory and experiment was also used [4] to probe the tautomerization of the ethylene phosphonate ion (**I**) into its phosphite and distonic counterparts **II** and **III**, which are lower in energy by 34 and 10 kcal/mol, respectively, see Scheme 1.

In brief, theory and experiment agree that low-energy phosphonate ions **I** readily tautomerize via a 1,2-H shift into phosphite ions **II**, prior to dissociation into $CH_2=CH_2^{\bullet+} + HOP(=O)_2$. This reaction dominates the metastable ion (MI) spectrum of both ions **I** and independently generated ions **II**. The tautomerization **I** → **III** has a much higher barrier, 32 kcal/mol, and the resulting energy-rich distonic ions readily undergo ring opening into the acyclic isomer $HO–CH_2–CH_2–O–P=O^{\bullet+}$.

Upon collisional activation, ions **I** and **II** show a pronounced loss of $CH_2=O$, as witnessed by an intense *m/z* 78 peak in their collision-induced dissociation (CID) mass spectra. Prominent *m/z* 78 ions are also observed in the electron impact (EI) mass spectra of **I** and ethyl ethylene phosphite, the precursor of **II**. Analysis of their CID spectra provides evidence that these *m/z* 78 ions are distonic ions $CH_2O–P–OH^{\bullet+}$ (**1b**) [5]. The spectra are characteristically different from those of the experimentally accessible isomers $CH_3O–P=O^{\bullet+}$ (**1a**) [5] and $CH_2=P(OH)=O^{\bullet+}$ (**1i**) the very stable enol tautomer of the elusive $CH_3–P(=O)_2^{\bullet+}$ ion (**1h**) [6].

The analysis of the CID spectra of the three $CH_3O_2P^{\bullet+}$ isomers is straightforward [5,6], but that of their MI spectra is not: the major dissociation of low-energy ions **1a** and **1b** appears to be a decarbonylation reaction, which requires a triple H-transfer for ions $CH_3O–P=O^{\bullet+}$. Metastable ions $CH_2=P(OH)=O^{\bullet+}$ (**1i**), also undergo decarbonylation but here loss of PO is more pronounced. A multiple collision experiment indicated that the resulting *m/z* 50 product ion is the as yet unknown ylide ion $H–P–OH_2^{\bullet+}$, rather than its more stable conventional isomer $H_2P–OH^{\bullet+}$. Further, an ^{18}O-labeling experiment revealed that the positional identity of the oxygen atoms in $CH_3O–P=O^{\bullet+}$ and $CH_2O–P–OH^{\bullet+}$ is lost in the decarbonylation. These observations prompted us to study the mechanism of this intriguing reaction, using the CBS-QB3 model chemistry to probe the structure and energetics of potential intermediates and their interconversion barriers. The metastable ions appear to have a substantial internal energy content: ca. 40 kcal/mol for ions **1b** and **1i** which represents the global minimum of the $CH_3O_2P^{\bullet+}$ potential energy surface. This broad energy domain comprises some 20 stable $CH_3O_2P^{\bullet+}$ isomers, including various ion–dipole complexes and hydrogen-bridged radical cations (HBRCs). Several of these, it will be shown, may account for the communication between metastable ions **1a**, **1b**, and **1i** and the oxygen

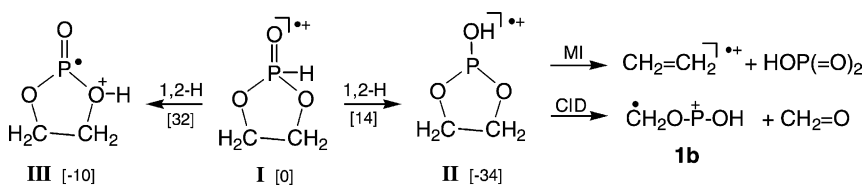

Scheme 1.

equilibration, whereas the HBRCs [O=CH(H)●●● P–OH]$^{\bullet+}$ and [O=C●●●H–O(H)–P–H]$^{\bullet+}$ appear to be key intermediates in the actual mechanism for the decarbonylation.

2. Experimental and theoretical methods

2.1. Sample preparation procedures

Methyl dichlorophosphate, $CH_3O–P(=O)Cl_2$, was obtained from Aldrich. The labeled isotopologues, $CH_3O^{18}–P(=O)Cl_2$ and $CH_2DO–P(=O)Cl_2$ were synthesized on a small scale by controlled methanolysis of $O=PCl_3$ [7]. In a typical experiment, 110 μl of $O=PCl_3$ (Aldrich) in 100 μl of dry ether was kept frozen in a small glass bulb using liquid N_2. Next, 25 μl of the labeled methanol in an equal volume of ether was transferred into the bulb with a syringe and frozen on top of the solid $O=PCl_3$/ether layer. The bulb was then quickly evacuated and, while pumping continuously with a rotary pump, the two layers were allowed to gradually come to room temperature over a period of ca. 1 h, using dry ice as the cooling agent. The resulting clear viscous liquid containing the desired isotopologue was sufficiently pure for our mass spectrometric experiments.

Ethylene phosphonate (1,3,2-dioxaphospholane, 2-oxide) and ethyl ethylene phosphite were obtained as described in reference [4]. Methyl hypophoshite, $CH_3O–P(H)_2=O$, was synthesized as described in [8] from a dehydrated 50% hypophosphorous acid/water solution (Aldrich) on the milligram scale. Methyl phosphonic acid, $CH_3–P(OH)_2=O$, was of research grade and obtained from Aldrich. The deuterium

Table 1a
Enthalpies of formation and relative energies, E_{rel} (kcal/mol) of the $CH_3O–P=O^{\bullet+}$ ion **1a**, and its principal isomers derived from CBS-QB3 calculations

Ion structure		E_{total} (0 K)[a]	ZPVE	ΔH_f° (0 K)	ΔH_f° (298 K)	E_{rel}[b]
$CH_3O–P=O^{\bullet+}$ (a)	**1a** (a)	−530.68346	27.89	137.9	135.4	14
	1a (s)	−530.68133	27.98	139.2	136.7	15
$CH_2O–P–OH^{\bullet+}$ (s/a)	**1b** (s/a)	−530.70506	26.91	124.4	121.5	0
	1b (s/s)	−530.69865	26.04	128.4	125.9	4.5
	1b (a/s)	−530.69905	26.30	128.1	125.5	4
	1b (a/a)	−530.69779	26.47	128.9	126.3	5
[HO–$P^{\bullet+}$●●●H–C(H)=O] (s)	HBRC-**1b** (s)	−530.65476	24.76	155.9	153.6	32
	HBRC-**1b** (a)	−530.64952	24.19	159.2	157.1	35.5
$CH_2O(H)–P=O^{\bullet+}$ (s)	**1c** (s)	−530.66664	25.86	148.5	146.5	25
	1c (a)	−530.66566	25.88	149.1	147.1	25.5
$[HO–CH_2]^+$●●●$O=P^\bullet$	ID-**1c**	−530.67735	28.76	141.7	139.1	17.5
$[CH_2–O–H^+$●●●$O=P^\bullet]$	HBRC-**1c**	−530.69034	26.77	133.6	131.1	9.5
$CH_2O–P(H)=O^{\bullet+}$	**1d**	−530.67567	25.83	142.8	140.1	18.5
$[–OCH_2O–]P–H^{\bullet+}$	**1e**	−530.67022	27.41	146.2	142.6	21
$[–OCH_2O(H)–]P^{\bullet+}$	**1f**	−530.67067	29.40	145.9	142.7	21
$H–C(=O)P(H)–OH^{\bullet+}$	**1g**	−530.67604	25.39	138.5	135.9	15
$[HO–PH]^+$●●●$O=CH^\bullet$	ID-**1g**	−530.65420	24.75	156.3	154.0	32.5
$CH_3–P(=O)_2^{\bullet+}$	**1h**	−530.65978	26.13	152.8	150.2	28
$CH_2=P(OH)=O^{\bullet+}$	**1i**	−530.70819	26.92	122.4	119.5	−2
$[–CH_2O–]P–OH^{\bullet+}$	**1j**	−530.68488	26.61	137.0	134.3	13
$HOCH_2–P=O^{\bullet+}$	**1k**	−530.67819	27.90	141.2	138.8	17.5
$HOCH=P(H)=O^{\bullet+}$	**1l**	−530.67264	26.99	144.7	141.7	20
$[HO–P(H)–H$●●●$C≡O]^{\bullet+}$	HBRC-**2a**	−530.69015	23.23	133.7	132.0	10.5
$[H–P–O(H)–H^{\bullet+}$●●●$C≡O]^{\bullet+}$	HBRC-**2b**	−530.68751	24.20	135.4	133.8	12.5
$[O=C=PH]^{\bullet+}$●●●OH_2	ID-**3b**	−530.69299	24.54	131.9	130.5	9
$[HO–PH_2]^{\bullet+}$●●●O≡C	ID-**2a**	−530.69194	23.39	132.6	130.9	9.5

[a] E_{total} in Hartrees, all other components, including the ZPVE scaled by 0.99, in kcal/mol.
[b] Using the ΔH_f° (298 K) value of the syn/anti isomer **1b** (s/a) as the anchor point.

isotopologue, CH_3–$P(OD)_2$=O, was obtained by repeated exchange with D_2O.

2.2. Tandem mass spectrometry

The tandem mass spectrometry-based experiments were performed with the McMaster University ZAB-R mass spectrometer, a three-sector BE_1E_2 (B = magnetic sector, E = electric sector) type instrument [9].

The compounds were introduced into the ion source (kept at 100 °C) via a wide-bore all-quartz direct insertion probe connected via an O-ring with a small glass bulb that contains the sample. Ions generated in the source by electron ionization (EI) were accelerated to 8 or 10 keV prior to recording their spontaneous or collision-induced dissociation in the second (2ffr) or the third field free (3ffr) regions as MI or CID spectra, respectively. The structure of a given product ion in a 2ffr MI or CID spectrum was probed by selectively transmitting the ion by E_1 to a collision chamber in the 3ffr pressurized with O_2 and mass-analyzing its ionic dissociation products by scanning E_2. All of the (high energy) collision experiments were performed at a main beam transmittance (~70%) such that the probability for multiple collisions is negligible. The

Table 1b
Enthalpies of formation and relative energies, E_{rel}, (kcal/mol) of transition states describing the isomerization and decarbonylation of the CH_3O–P=$O^{\bullet+}$ ion **1a**, and its principal isomers derived from CBS-QB3 calculations

	E_{total} (0 K)[a]	ZPVE	ΔH_f° (0 K)	ΔH_f° (298 K)	E_{rel}[b]
TS **1a** → **1b** (s/s)	−530.65170	27.98	160.0	156.8	35.5
TS **1a** → **1c**	−530.60896	25.86	184.7	182.1	60.5
TS **1a** → **1d**	−530.62240	24.67	176.2	173.1	51.5
TS **1a** (a) → **1h**	−530.62144	25.78	176.8	174.3	53
TS **1a** (1,3-CH_3)	−530.62178	25.34	176.6	174.1	52.5
TS **1b** (s/s → s/a)	−530.69770	25.87	129.0	126.1	4.5
TS **1b** → HBRC-**1b**	−530.65015	24.93	158.8	156.1	34.5
TS **1b** → HBRC-**1c**	−530.67052	26.25	146.0	143.4	22
TS **1b** → **1d**	−530.62551	23.82	174.3	171.6	50
TS **1b** → **1f**	−530.65792	27.74	153.9	150.6	29
TS **1b** → **1j**	−530.67615	25.47	142.5	139.7	18
TS **1d** → HBRC-**1c**	−530.63675	23.23	167.2	164.9	43.5
TS **1d** → **1e**	−530.63511	25.67	168.2	164.8	43.5
TS **1e** → **1f**	−530.61447	25.72	181.2	177.6	56
TS **1f** → ID-**1c**	−530.66233	28.90	151.2	147.7	26
TS **1h** → **1i**	−530.62154	26.08	176.8	173.0	51.5
TS HBRC-**1b** → **1g**	−530.64621	23.49	161.3	158.8	37.5
TS **1g** → HBRC-**2a**	−530.64681	23.19	160.9	158.9	37.5
TS **1g** → HBRC-**2b**	−530.65828	23.62	153.7	151.1	29.5
TS HBRC-**1b** (s → a)	−530.64900	24.25	159.5	156.9	35.5
TS HBRC-**1b** → HBRC-**1c**	−530.65473	25.04	155.9	153.2	31.5
TS ID-**1c** → HBRC-**1c**	−530.67116	27.60	145.6	143.0	21.5
TS HBRC-**1b** → HBRC-**2b**	−530.65099	23.40	158.3	155.7	34
TS HBRC-**2b** → ID-**3b**	−530.67185	23.67	145.2	143.8	22.5
TS **1i** (1,3-H)	−530.63003	23.77	171.4	168.4	47
TS **1i** → **1j**	−530.63765	25.69	166.7	163.7	42
TS **1i** → **1k**	−530.62433	28.94	175.0	171.5	50
TS **1k** → HBRC-**1c**	−530.66656	27.45	148.5	145.7	24
TS **1k** → **1l**	−530.61857	25.02	178.6	174.9	53.5
TS **1g** → **1l**	−530.65832	24.29	153.7	150.2	28.5

[a] E_{total} in Hartrees, all other components, including the ZPVE scaled by 0.99, in kcal/mol.
[b] Using the ΔH_f° (298 K) value of the syn/anti isomer **1b** (s/a) as the anchor point.

Table 1c
Relative energies, E_{rel} (kcal/mol), of dissociation reactions of ion **1b** derived from CBS-QB3 calculations

Dissociation products	*m/z*	E_{rel} (298 K)[a]
$CH_2O–P{=}O^+ + H^\bullet$	77	51
$[–OCH_2O–]P^{\bullet+} + H^\bullet$	77	51
$O{=}P–OH^{\bullet+} + CH_2^{\bullet\bullet}$	64	125
$P–OCH_3^{\bullet+} + O$	62	123
$CH_2{=}P–OH^{\bullet+} + O$	62	118
$HPCO^{\bullet+} + H_2O$	60	25
$[–OC(H)–]P^{\bullet+} + H_2O$	60	52
$HCPO^{\bullet+} + H_2O$	60	96
$H_2POH^{\bullet+} + CO$	50	14
$H–P–OH_2^{\bullet+} + CO$	50	24
$P–OH^{\bullet+} + CH_2{=}O$	48	43
$H–P{=}O^{\bullet+} + CH_2{=}O$	48	67
$PO^+ + CH_2OH^\bullet$	47	59
$CH_2–OH^+ + PO^\bullet$	31	39
$HCO^+ + HPOH^\bullet$	29	51

[a] Using the ΔH_f° (298 K) value of the syn/anti isomer **1b** (s/a) as the anchor point.

quoted kinetic energy releases refer to $T_{0.5}$ values derived from the width at half-height of the appropriate metastable peak, by means of the standard one-line equation, with no correction for the width of the main beam [10]. All spectra were recorded using a small PC-based data system developed by Mommers Technologies Inc. (Ottawa).

2.3. Computational procedures

The calculations were performed using Gaussian 98 Revision A.9 [11]. The standard CBS-QB3 model chemistry [3] was used to probe structures and energies of the key isomeric ions, connecting transition states and dissociation products associated with the $CH_3O_2P^{\bullet+}$ potential energy surface. The energetic results are presented in Tables 1a and b (equilibrium and transition state energies), Table 1c (dissociation products) and Schemes 2, 7and 8. In the schemes, the energy levels for the minima and transition states are represented by solid and dashed lines, respectively. Detailed geometries of selected species are displayed in Figs. 1 and 2 (the complete set of geometries is available upon request). Frequency calculations gave the correct number of negative eigenvalues for all minima and transition states and the spin contamination was within the acceptable range. The connections of the transition states have been checked by geometry optimizations and frequency calculations.

Several of the isomeric ions studied were found to have stable conformers, like ion **1b** whose four conformers are shown in Fig. 1. The various conformers are listed in Tables 1a–c and Figs. 1 and 2 using a syn (s)/anti (a) notation where we start viewing the C–O bond and move towards the O–H bond in the assignment. For example, in conformer **1b** (s/a) the C atom is on the same side of the $CH_2O–P$ bond as the hydroxylic O atom, designated as "syn," whereas the CO oxygen is on the opposite side of the P–OH bond to the H atom, designated as "anti." Among the conformers of **1b**, the (s/a) conformer is the most stable, by ca. 5 kcal/mol. Since the interconversion barriers are relatively low, ca. 5 kcal/mol (Table 1a), the conformers are collectively referred to as **1b** in the text and the energy diagrams.

3. Results and discussion

3.1. The dissociation characteristics of ions *1a*, *1b*, and *1i*

We will begin our analysis of the results with a brief survey of the spontaneous and collision-induced dissociation characteristics of the experimentally accessible $CH_3O_2P^{\bullet+}$ isomers $CH_3O–P{=}O^{\bullet+}$ (**1a**) $CH_2O–P–OH^{\bullet+}$ (**1b**) and $CH_2{=}P(OH){=}O^{\bullet+}$ (**1i**) using the energetic information presented in Tables 1a–c and the simplified energy diagram of Scheme 2 as a guide. The CID and MI spectra of the three isomeric ions and selected isotopologues are presented in Figs. 3 and 4.

Ion **1a** was generated from $CH_3O–P(=O)Cl_2^{\bullet+}$, by the consecutive loss of two $Cl^\bullet$ radicals, as discussed in [5], while ion **1b** was obtained from the cyclic precursor ions of Scheme 1 (see Section 1). As seen in Scheme 2, the distonic ion **1b** is more stable than its H-shift isomer of conventional structure **1a**. The two ions can communicate via a 1,4-H shift at internal

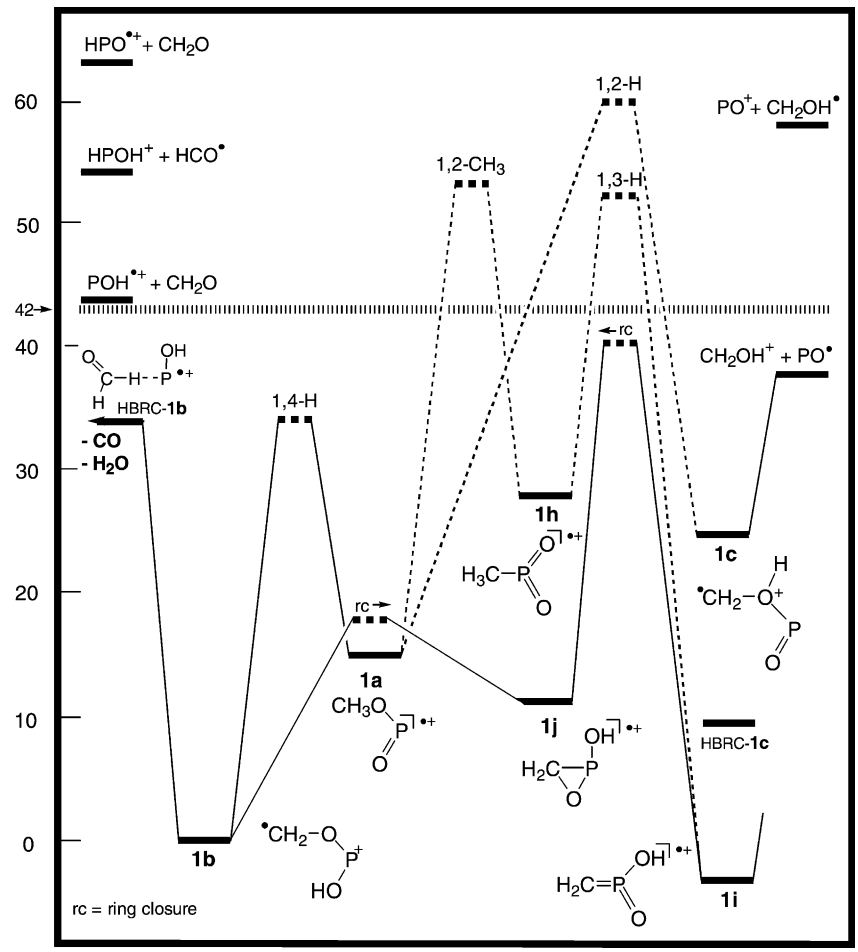

Scheme 2. Potential energy diagram derived from CBS-QB3 (298 K, Tables 1a–c) calculations describing the isomerization reactions of the CH_3O_2P ions $CH_3O–P=O^{\bullet+}$ (**1a**), $CH_2O–P–OH^{\bullet+}$ (**1b**) and $CH_2=P(OH)=O^{\bullet+}$ (**1i**). All energies, in kcal/mol, are relative to **1b**.

energies below that required for dissociation into *m/z* 31 (CH_2OH^+), *m/z* 48 ($POH^{\bullet+}$) and *m/z* 47 (PO^+). These reactions dominate the CID spectra (see Fig. 3) and it is therefore not surprising that these spectra are similar (the sizable peak at *m/z* 50 in the CID spectrum of **1a** is largely of metastable origin). Nevertheless, the CID spectra do contain tell-tale peaks, at *m/z* 62 and 64, which attests to the structure identity of the two isomers. Analysis of the collision-induced dissociative ionization (CIDI; [12]) spectrum of neutral $CH_3O–P=O$ [5] confirms that the high energy dissociation $CH_3O–P=O^{\bullet+} \rightarrow CH_3OP^{\bullet+}$ (*m/z* 62) + O is a characteristic feature of the CID spectrum of ion **1a**. Its H-shift isomer **1b** is characterized by another high energy process viz. $CH_2O–P–OH^{\bullet+} \rightarrow O=P–OH^{\bullet+}$ (*m/z* 64) + CH_2 and also a prominent charge stripping peak at *m/z* 39. The MI spectra of the two isomers (see Fig. 4) are dominated by loss of CO. The kinetic energy release associated with this reaction, $T_{0.5}$ = 40 meV, is the same for both isomers. This suggests that the energy requirement for the decarbonylation is higher than that for the interconversion of **1a** and **1b**. Loss of H_2O is a minor process but, especially for **1b**, dissociation into CH_2OH^+ (*m/z* 31) + $PO^{\bullet}$ is more pronounced. The associated small $T_{0.5}$ value (18 meV) suggests that the dissociation

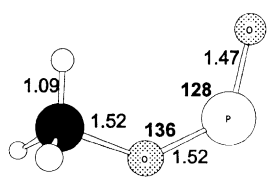

1a (syn)

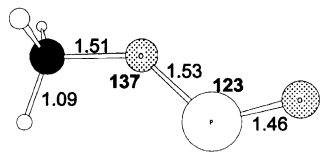

1a (anti)

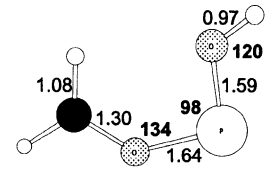

1b (s/a)

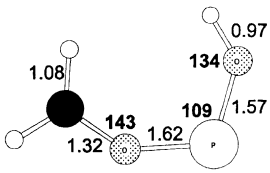

1b (s/s)

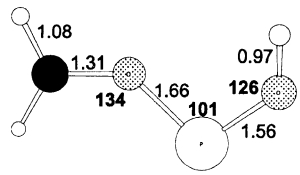

1b (a/s)

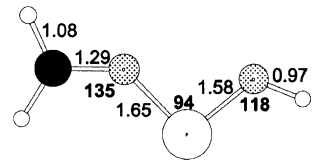

1b (a/a)

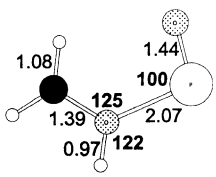

1c (syn)

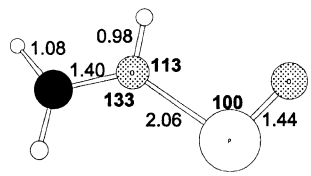

1c (anti)

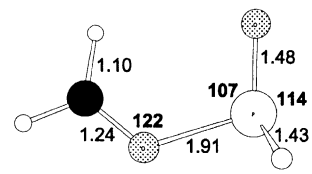

1d

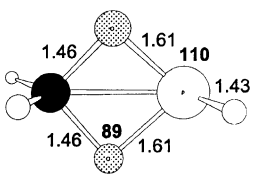

1e

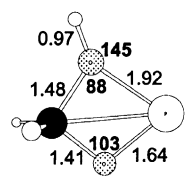

1f

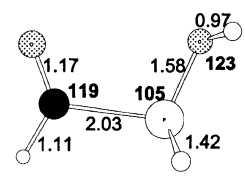

1g (syn)

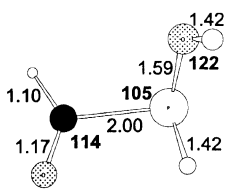

1g (anti)

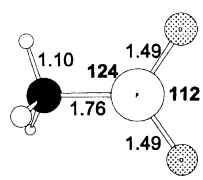

1h

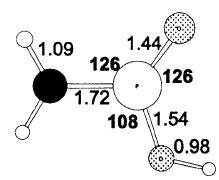

1i

Fig. 1. Optimized geometries of the various isomers of the $CH_3O–P=O^{\bullet+}$ ion (**1a**). The bond lengths (Å) and angles are presented in normal and bold font, respectively.

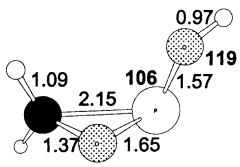

1j

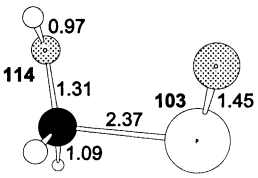

1k

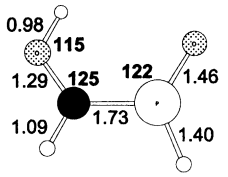

1l

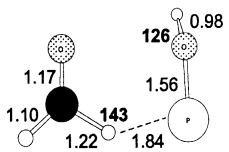

HBRC-1b (syn)

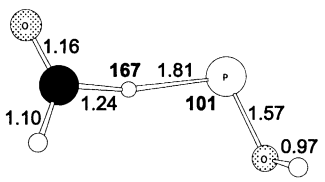

HBRC-1b (anti)

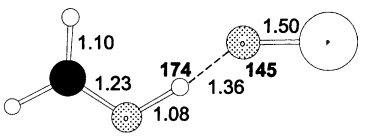

HBRC-1c

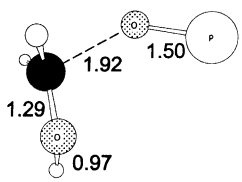

ID-1c

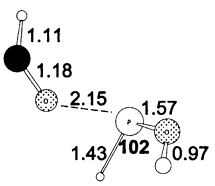

ID-1g

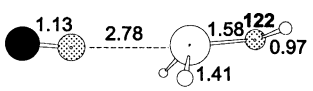

ID-2a

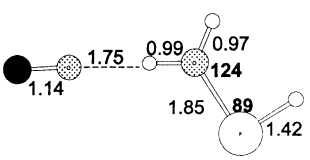

ID-2b

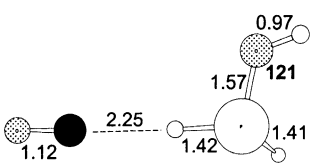

HBRC-2a

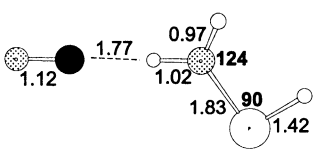

HBRC-2b

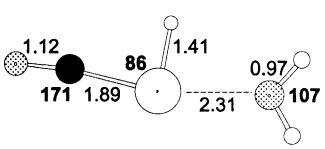

ID-3b

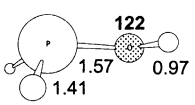

H_2P-OH$^{\bullet+}$

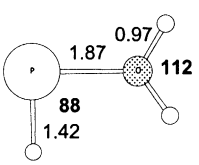

HP-$OH_2^{\bullet+}$

Fig. 1. (*Continued*).

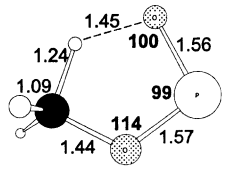

TS 1a - 1b (s/s)

TS 1a - 1c

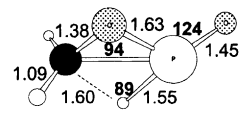

TS 1a - 1d

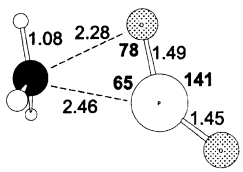

TS 1a (a) - **1h**

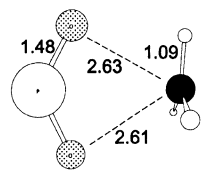

TS 1a - 1a

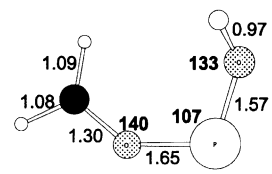

TS 1b - 1b

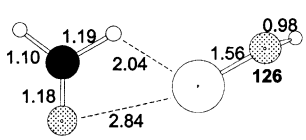

TS 1b - HBRC-1b

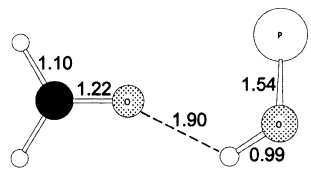

TS 1b - HBRC-1c

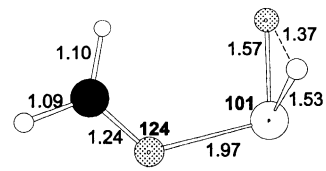

TS 1b - 1d

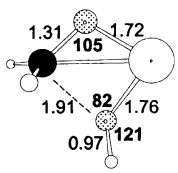

TS 1b - 1f

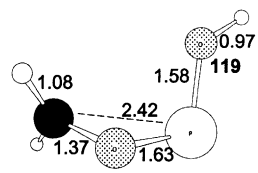

TS 1b - 1j

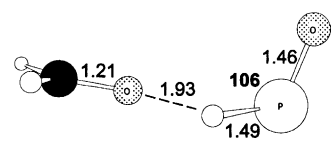

TS 1d - HBRC-1c

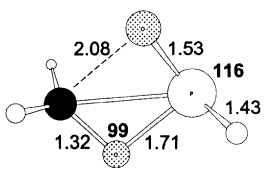

TS 1d - 1e

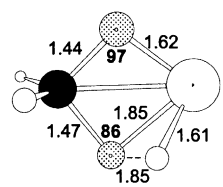

TS 1e - 1f

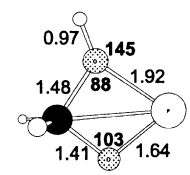

TS 1f - ID-1c

Fig. 2. Optimized geometries of the transition states connecting the various isomers of the $CH_3O–P=O^{\bullet+}$ ion (**1a**). The bond lengths (Å) and angles are presented in normal and bold font, respectively.

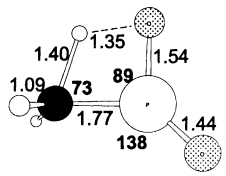

TS 1h - 1i

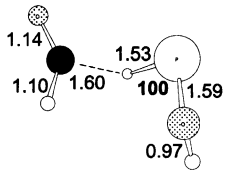

TS HBRC-1b - 1g

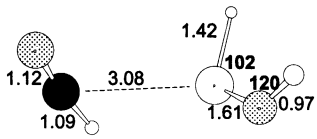

TS 1g - HBRC-2a

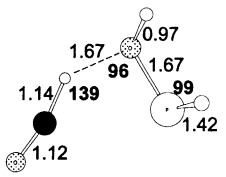

TS 1g - HBRC-2b

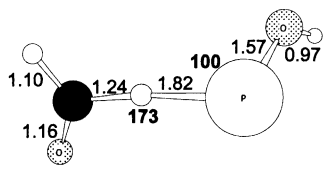

TS HBRC-1b - HBRC-1b

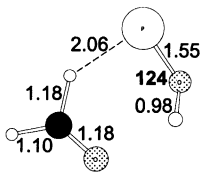

TS HBRC-1b - HBRC-1c

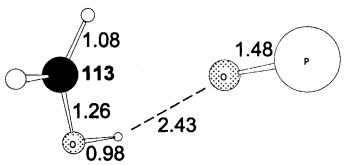

TS ID-1c - HBRC-1c

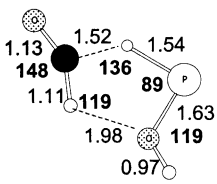

TS HBRC-1b - HBRC-2b

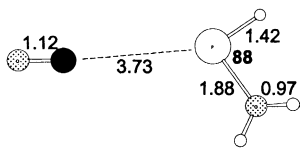

TS HBRC-2b - ID-3b

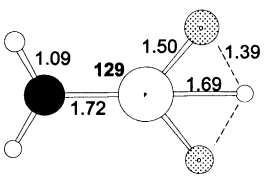

TS 1i - 1i

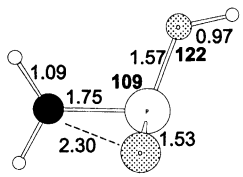

TS 1i - 1j

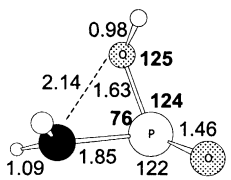

TS 1i - 1k

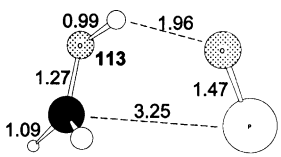

TS 1k - HBRC-1c

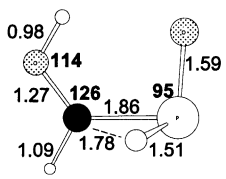

TS 1k - 1l

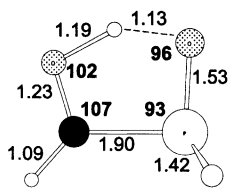

TS 1g - 1l

Fig. 2. (*Continued*).

CH_2O–P–$OH^{\bullet+}$ → CH_2OH^+ + $PO^{\bullet}$ takes place at or close to the thermochemical threshold.

As shown in [6], ionized methyl phosphonic acid, CH_3–$P(OH)_2$=$O^{\bullet+}$, readily loses H_2O to cleanly generate the "enol" ion CH_2=P(OH)=$O^{\bullet+}$ (**1i**) rather than its "keto" tautomer CH_3–$P(=O)_2{}^{\bullet+}$ (**1h**). This is because the enol ion is much lower in energy: ion **1h** is the highest energy isomer on the $CH_3O_2P^{\bullet+}$ PES, whereas its enol counterpart represents the global minimum (see Table 1a and Scheme 2). Ion **1h** has been

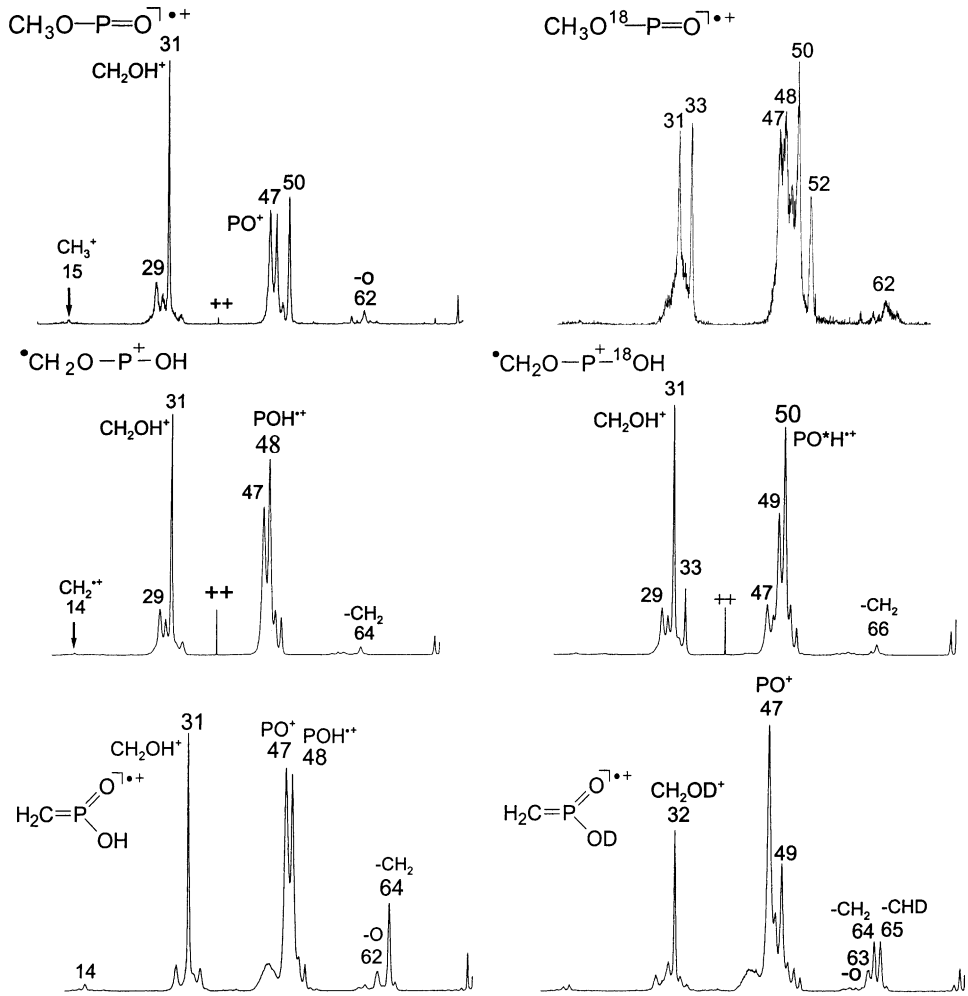

Fig. 3. CID spectra of *m/z* 78 ions (left): **1a** (top), **1b** (middle), and **1i** (bottom) and their ^{18}O- and D-labeled isotopologues (right).

identified as a stable species in a CIDI experiment of its neutral counterpart [6]. However, considering the high isomerization barriers (see Scheme 2) this ion clearly plays no role in the dissociation chemistry of metastable ions **1i** and **1a**/**b**.

The CID spectrum of **1i**, CH_2=P(OH)=O$^{\bullet+}$ displays structure characteristic peaks for the high energy losses of CH_2 (*m/z* 64) and O (*m/z* 62). Collision experiments involving neutralization–reionization mass spectrometry [13] indicate that non-dissociating ions **1i** retain their structure identity. This too, is in agreement with the energy diagram of Scheme 2, which shows that the ions lie in a deep potential well with high barriers towards isomerization. However, upon collisional activation some isomerization does occur. It can be seen from the CID mass spectrum of **1i**-OD (see Fig. 3) that the high energy loss of CH_2 is split into losses of CH_2 and CHD. Thus, amongst the higher energy ions communication of **1i** with **1a** is possible (see Scheme 2). Fig. 4 shows that metastable ions **1i** are less prone to decarbonylate than **1a**/**b**, while loss of H_2O hardly takes place at all. The kinetic energy release for loss of CO ($T_{0.5}$ = 40 meV) is the same as that for ions **1a**/**b**, while that for loss of PO$^{\bullet}$ into

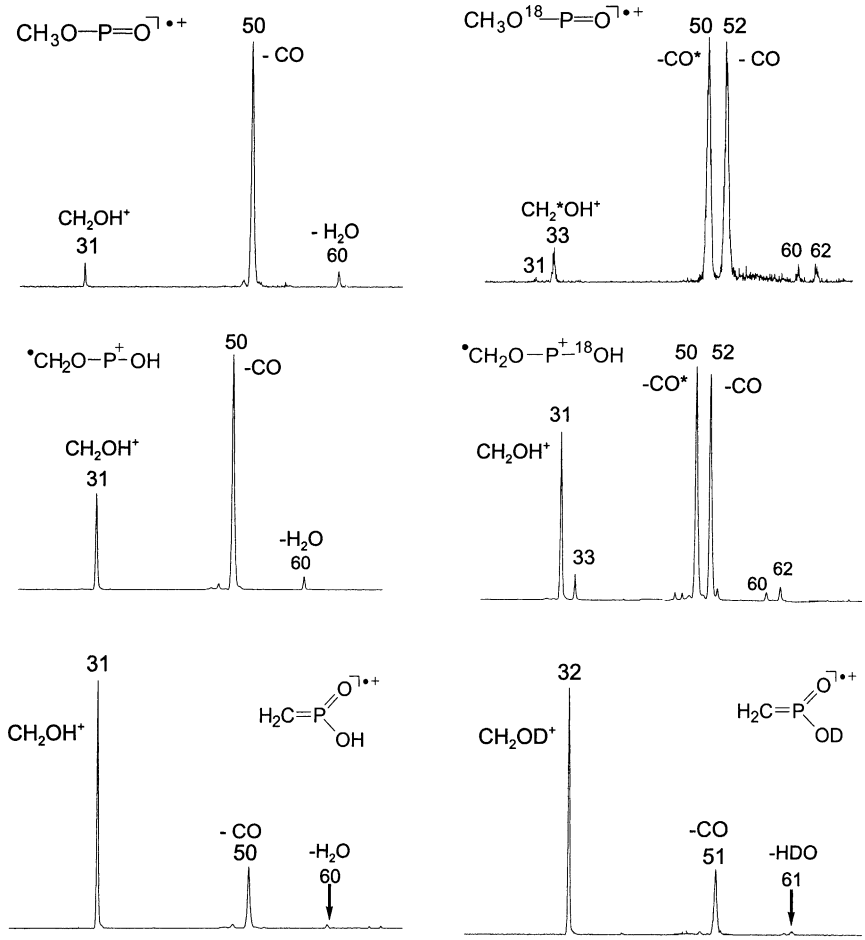

Fig. 4. MI spectra of *m/z* 78 ions (left): **1a** (top), **1b** (middle), and **1i** (bottom) and their ^{18}O- and D-labeled isotopologues (right).

CH_2OH^+ is smaller, $T_{0.5} = 10$ meV. These observations indicate that (see Scheme 2) the small fraction of metastable ions **1i** that undergo decarbonylation does so by entering the potential energy-surface populated by ions **1a**/**b**, via the energy demanding ring closure that leads to ion **1j**. The majority of the ions generate CH_2OH^+, possibly by an extrusion reaction, at or close to the thermochemical threshold. The energy required for the degenerate 1,3-H shift of the hydroxylic hydrogen atom is high (TS **1i**–**1i** in Table 1b) which indicates that ion **1i** plays no role in the oxygen equilibration of ^{18}O-labeled ions **1a**/**b** discussed below.

Dissociation into $CH_2OH^+ + PO^\bullet$ accounts for the common base peak at *m/z* 31 in the CID spectra of the three isomers. Metastable ions **1a**, **1b**, and **1i** also undergo this rearrangement reaction, albeit to a different extent. Its calculated minimum energy requirement is only slightly lower (by 4 kcal/mol, see Table 1c) than that for dissociation into $POH^{\bullet+}$ (*m/z* 48) + CH_2=O. The latter reaction involves a simple bond cleavage in ion **1b**, requiring 43 kcal/mol of internal energy. Yet, although featuring prominently in the CID spectra, loss of CH_2=O is barely detectable in the MI spectra of all three isomers (see Fig. 4). This implies that the internal energy of metastable ions **1b**, and probably also that of **1a** and **1i**, does not exceed the value represented by the hatched line that bisects the energy diagram of Scheme 2 at ca. 42 kcal/mol. Consequently,

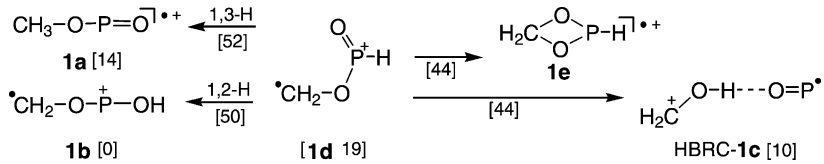

Scheme 3.

computationally derived proposals for the isomerization and dissociation pathways of metastable ions **1a**, **1b**, and **1i** must not have steps whose transition state energies lie above the hatched line in the energy diagrams of Schemes 2, 7 and 8. By the same token, metastable ions **1a** and **1b** cannot dissociate into $CH_2OH^+ + PO^\bullet$ via the pathway **1b** → **1a** → **1c** → products, because the 1,2-H shift connecting **1a** and **1c** is prohibitively high (see Scheme 2). However, ion **1c** has a low lying isomer, the hydrogen-bridged radical cation HBRC-**1c**, [$^+CH_2O$–H•••O=P$^\bullet$], whose generation from **1b** involves only a modest barrier (Table 1b) and which may serve as the direct precursor for the formation of CH_2OH^+. As we shall see in Section 3.3, HBRC-**1c** plays a key role in our proposed mechanism of the decarbonylation reaction.

Two more points deserve to be mentioned with regard to ion **1b**:

(i) The internal energy available to metastable ions **1b** is only marginally lower than that required for formation of $POH^{\bullet+}$ by cleavage of the CH_2O–POH bond. Therefore, lengthening of this bond may well be feasible, allowing metastable ions **1b** to form ion–dipole complexes of the type [POH•••O=CH_2]$^{\bullet+}$. Internal rotations will allow these ions to adopt configurations which are best described as hydrogen-bridge radical cations. One such species, which has been calculated to lie in a shallow well, is HBRC-**1b** in Scheme 2. It has an ideal configuration for H-abstraction from its CH_2=O component that could eventually lead to decarbonylation. As will be discussed in Section 3.3, HBRC-**1b** is indeed a key player in the decarbonylation of the metastable ions.

(ii) As stated in Section 1, ionized ethylene phosphonate, **I**, cleanly generates ions **1b**, via the route **I** → **II** → **1b** (*m*/*z* 78) + CH_2O, as depicted in Scheme 1. A direct loss of CH_2O from **I** would yield ions of structure $CH_2OP(H)=O^{\bullet+}$ (**1d**) which are 19 kcal/mol higher in energy than **1b**. There is no evidence that this ion is (co)generated from **I** as the CID spectra of the source- and metastably-generated *m*/*z* 78 ions from **I** and **II** are virtually identical. However, ion **1d** could still play a role in the decarbonylation mechanism if its isomerization barriers are sufficiently low. Scheme 3 summarizes four potential isomerization routes for ion **1d**, and it is seen that their energies (numbers between brackets) are too high for effective communication with metastable ions **1a**/**b**.

As mentioned before, and shown in Fig. 4, the ^{18}O-labeled isotopologues CH_3O^{18}–P=O$^{\bullet+}$ and CH_2O–P–$^{18}OH^{\bullet+}$ lose CO and CO^{18} in a 1:1 ratio. The positional identity of the oxygen atoms is also lost in the minor loss of H_2O, but not in the loss of PO$^\bullet$.

Neither of the two simple transformations depicted in Scheme 4 can account for the loss of positional identity of the oxygen atoms in the decarbonylation of metastable ions **1a**/**b**. The pathway **1a** ⇌ **1b** ⇌ **1f** is energetically feasible but the ensuing 1,2-H shift connecting the cyclic ions **1f** and **1e** is clearly too high in energy. This is also true for the degenerate 1,3-CH_3 shift in ion **1a**, although this process could account for the closely similar intensities of the *m*/*z* 31 ($CH_2{}^{16}OH^+$) and *m*/*z* 33 ($CH_2{}^{18}OH^+$) peaks in the CID spectrum of CH_3O^{18}–P=O$^{\bullet+}$.

Nevertheless, the remarkably stable cyclic ion **1f** plays a key role in a pathway that does account for the loss of the positional identity of the oxygen atoms in the decarbonylation of ions **1a**/**b**. This is depicted in Scheme 5 where the asterisk

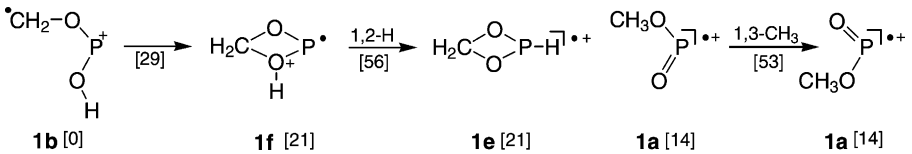

Scheme 4.

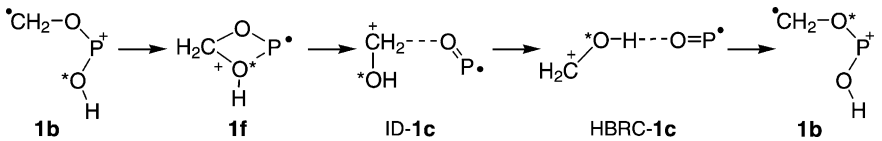

Scheme 5.

is used to indicate the position of the ^{18}O-labeled atom.

A cursory inspection of the energy diagram of Scheme 8 shows that that this sequence of reactions is energetically feasible. A more detailed analysis will be presented in Section 3.3. In the next section, we will first examine the evidence for the structure of the product ion generated in the decarbonylation reaction and also the accompanying minor loss of water.

3.2. The identification of the product ions of the decarbonylation and the H_2O loss

The decarbonylation process generates *m/z* 50 ions of putative structure $H_2P–OH^{\bullet+}$ or $H–P–OH_2^{\bullet+}$. The calculated energy levels depicted in Scheme 8 indicate that both product ions could in principle be generated. The ylide ion $H–P–OH_2^{\bullet+}$ is 10 kcal/mol less stable than its conventional isomer $H_2P–OH^{\bullet+}$ but the two ions cannot easily interconvert: the calculated barrier for the appropriate 1,2-H shift is high, 51 kcal/mol.

The CID spectra of the *m/z* 50 ions generated from metastable ions **1a**, **1b**, and **1i** are virtually identical, and a representative spectrum is presented in Fig. 5 (top). This spectrum displays a prominent peak at *m/z*

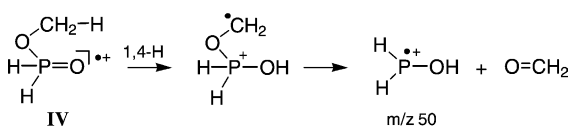

Scheme 6.

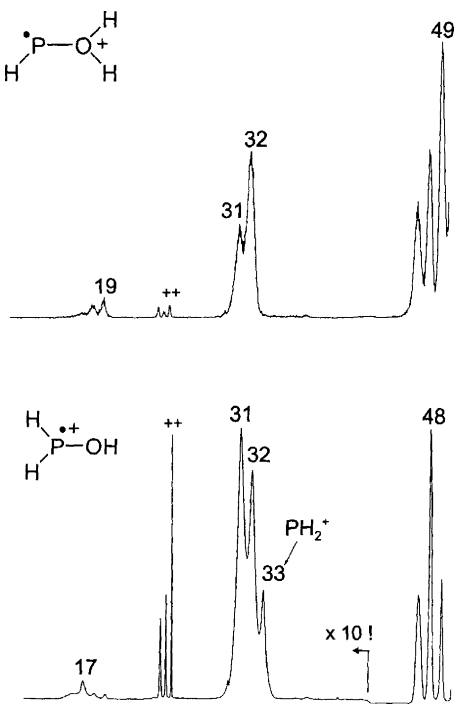

Fig. 5. CID spectra of *m/z* 50 ions generated from: Metastable ions **1b** (top) and ionized methyl phosphonic acid (bottom).

32 for loss of H_2O, but there is no peak at *m/z* 33 for loss of $OH^{\bullet}$. This suggests that we are dealing with the ylide ion $H–P–OH_2^{\bullet+}$ rather than $H_2P–OH^{\bullet+}$. The latter isomer could be generated independently from ionized methyl phosphinate, **IV**, by the route depicted in Scheme 6.

The CID spectrum of the so generated *m/z* 50 ions (see Fig. 5 (bottom)) shows a prominent tell-tale peak

at *m/z* 33 (loss of $OH^{\bullet}$) and even a weak *m/z* 17 (OH^{+}) ion, indicative of the $H_2P–OH^{\bullet+}$ structure. This supports our proposal that the decarbonylation of the three isomers results in the formation of the ylide ion $H–P–OH_2^{\bullet+}$. It can also be seen that the conventional isomer shows an intense and characteristically narrow peak for the formation of the doubly charged species $H_2P–OH^{2+}$, while that for the ylide ion $H–P–OH_2^{2+}$ is relatively weak, the opposite of what is usually encountered [14].

The minor H_2O loss from the metastable ions yields *m/z* 60 ions of structure $H–P=C=O^{\bullet+}$. The calculations predict that among the family of stable [C/H/P/O] ions, only $H–P=C=O^{\bullet+}$ is sufficiently low in energy to be generated from the metastable ions (see Scheme 8 and Table 1c). Confirmation of the proposed ion structure comes from the CID spectrum of the *m/z* 60 ions generated from the metastable *m/z* 78 ions. The spectrum (not shown) displays fairly intense structure characteristic peaks at *m/z* 28 and 32 corresponding to $CO^{\bullet+}$ and $HP^{\bullet+}$, agreeing with the proposed $HPCO^{\bullet+}$ ion structure.

3.3. Mechanistic proposals for the decarbonylation of the $CH_3O–P=O^{\bullet+}$ and $CH_2O–P–OH^{\bullet+}$ ions and mechanism for the oxygen exchange reaction

3.3.1. Mechanism for decarbonylation

As indicated in Scheme 7, HBRC-**1b** is accessible from ions **1b** having ≥35 kcal/mol of internal energy.

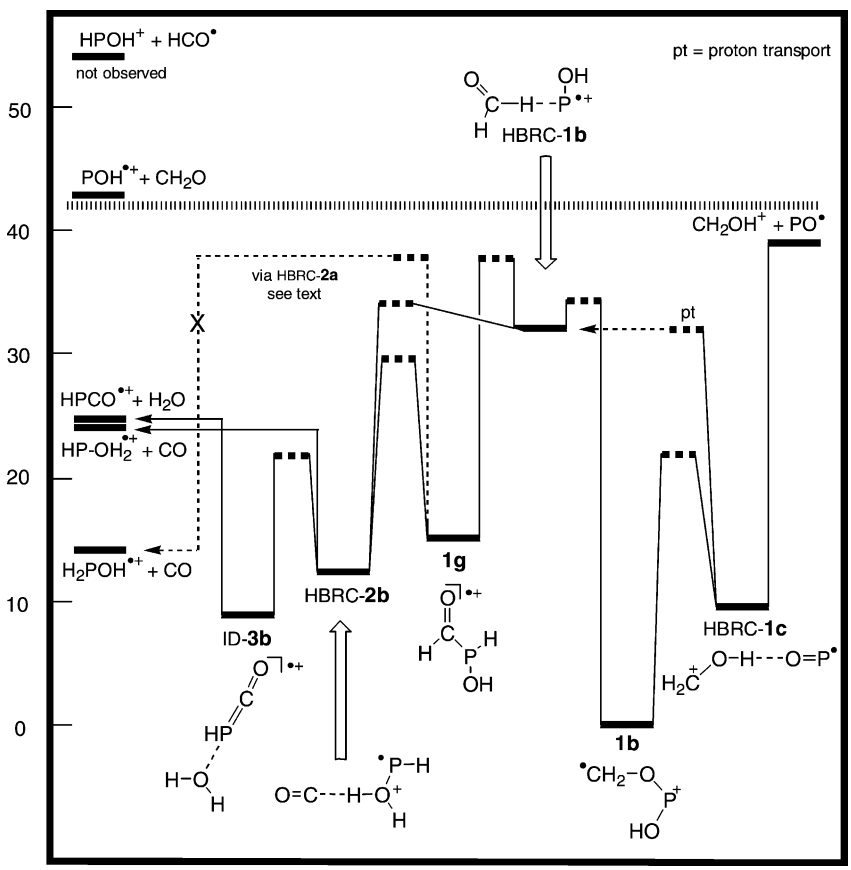

Scheme 7. Potential energy diagram derived form CBS-QB3 (298 K, Tables 1a–c) calculations describing the decarbonylation and water loss from metastable ions $CH_2O–P–OH^{\bullet+}$ (**1b**) and related isomers.

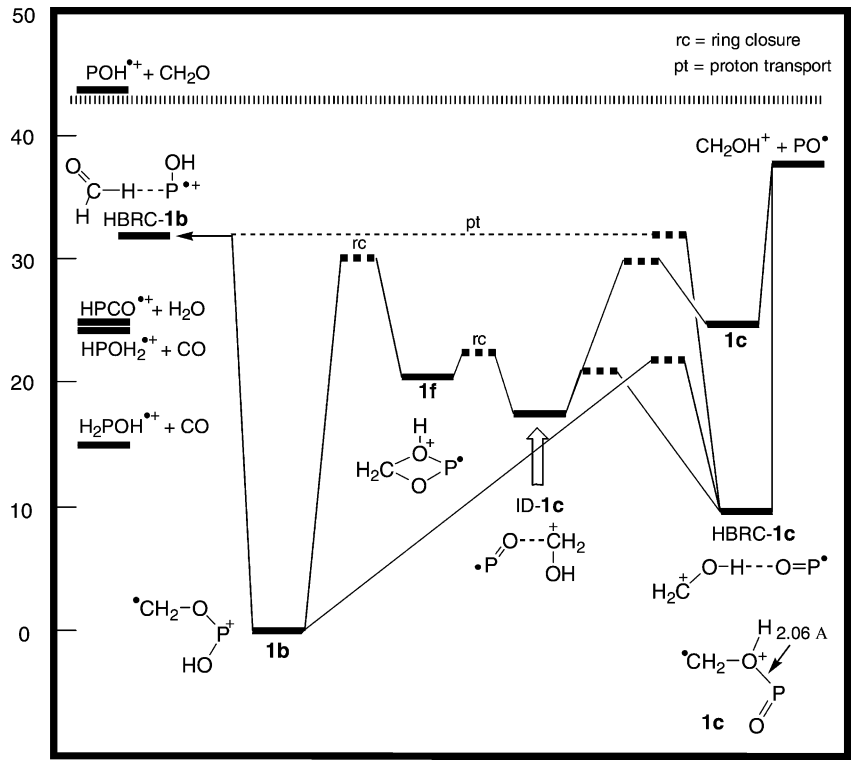

Scheme 8. Potential energy diagram derived form CBS-QB3 (298 K, Tables 1a–c) calculations describing the isomerization reactions of metastable ions [CH_2O–P–$OH^{\bullet+}$] which may lead to the oxygen equilibration prior to decarbonylation and loss of water.

At this energy, HBRC-**1b** can communicate with HBRC-**2b**, which may dissociate into H–P–$OH_2^{\bullet+}$ and CO by direct bond cleavage. Alternatively, ions HBRC-**1b** with a slightly lower internal energy, 32 kcal/mol, can be formed from HBRC-**1c** via a proton transfer. Such ions can access HBRC-**2b** with 34 kcal/mol of internal energy relative to **1b**. Thus, the calculated minimum energy requirement for the observed decarbonylation into the ylide ion $HPOH_2^{\bullet+}$ is 34 kcal/mol.

Our experiments show that the lower energy isomer H_2P–$OH^{\bullet+}$ is not formed as a result of decarbonylation. Theory indicates that this is so because the formation of the immediate precursor to H_2P–$OH^{\bullet+}$, viz. HBRC-**2a**, [HO–P(H)–H•••C=O]$^{\bullet+}$, which is 2 kcal/mol lower in energy than HBRC-**2b**, is energetically unfavorable. HBRC-**1b** cannot directly communicate with HBRC-**2a**: it must first isomerize into the relatively stable ion **1g**, H–C(=O)P(H)–$OH^{\bullet+}$, which involves a barrier of 5, or 38 kcal/mol relative to **1b**. (There is also an ion–dipole complex of **1g**, [HO–PH^+]•••O=$CH^{\bullet}$, which, see Table 1a, lies 17.5 kcal/mol above **1g**.) This barrier is of the same height as that for the subsequent isomerization of **1g** into HBRC-**2a**. However, metastable ions **1b** having more than 38 kcal/mol of internal energy can also dissociate via the route **1b** → HBRC-**1c** → $CH_2OH^+ + PO^{\bullet}$. This clearly is a fast rearrangement reaction—it effectively competes with direct bond cleavage into $POH^{\bullet+}$ in collisionally energized ions **1b**—which discriminates against the slow multi-step decarbonylation route.

The HBRC-**2b** ion is the direct precursor for loss of CO and a key intermediate for the H_2O loss. Cleavage

of the weak C●●●H bond in HBRC-**2b** results in the formation of $HP–OH_2^{\bullet+} + CO$. Just below the threshold for decarbonylation (see Scheme 7) HBRC-**2b** can also rearrange into ID-**3b**, $[O=C=PH]^{\bullet+}●●●OH_2$, which can dissociate into $HP=C=O^{\bullet+} + H_2O$ by simple cleavage. The minimum energy requirement for this reaction is very close to that of the decarbonylation reaction. However, loss of H_2O requires formation of two new covalent bonds in the loosely bound ion–dipole complex HBRC-**2b** to form the ion–dipole complex ID-**3b** and so "hot" HBRC-**2b** ions, having about 14 kcal/mol excess energy will preferentially undergo a simple cleavage reaction, i.e., loss of CO. Furthermore, as the dipole moment of CO is very small, it is not surprising that the complex prefers dissociation over rearrangement. These matters explain that compared to loss of CO, the loss of H_2O is a minor process in the dissociation of metastable ions.

One important point should be considered regarding HBRC-**2b**, $[H–P–O(H)–H●●●CO]^{\bullet+}$. This ion can be considered as an encounter complex between a $HP–OH_2^{\bullet+}$ ion and a CO molecule. In such an encounter complex the neutral molecule may promote the tautomerization of the ionic component by lowering the barrier for the associated H-transfer. This phenomenon, termed proton-transport catalysis by Böhme [15], has been demonstrated in several ionic systems [1]. For example, the isomerization of $HCN^{\bullet+}$ into its more stable $HNC^{\bullet+}$ tautomer does not occur spontaneously because the barrier for the associated 1,2-H shift is too high, 27 kcal/mol. However, in the presence of CO, the tautomerization readily takes place in the encounter complex, via: $CO + HCN^{\bullet+} \rightarrow OC●●H^{+}●●[C≡N]^{\bullet} \rightarrow [C≡N]^{\bullet}●●H^{+}●●CO \rightarrow HNC^{\bullet+} + CO$, and the barrier becomes vanishingly small. This system satisfies the criterion proposed by Radom and co-workers [1a] for effective proton-transport catalysis. It stipulates that the proton affinity (PA) of the neutral molecule in the encounter complex (PA CO at C) must lie in between those of the two protonation sites in the deprotonated ion (PA $CN^{\bullet}$ at C and N, respectively).

By analogy, the CO molecule in HBRC-**2b** could promote the tautomerization of $HP–OH_2^{\bullet+}$ into $H_2P–OH^{\bullet+}$, via $[HP–OH]^{\bullet}●●H^{+}●●CO$ (HBRC-**2b**)→ $OC●●H^{+}●●[HP–OH]^{\bullet}$ (HBRC-**2a**) → $H_2P–OH^{\bullet+} + CO$, if the criterion for proton-transport catalysis is satisfied. This implies that PA CO at C, 142 kcal/mol [16a], be in between PA $HP–OH^{\bullet}$ at O and PA $HP–OH^{\bullet}$ at P. From the enthalpies of formation of $HP–OH^{\bullet}$, $H_2P–OH^{\bullet+}$ and $HP–OH_2^{\bullet}$ (−24.7, 162.7 and 172.5 kcal/mol, respectively, [16b]), we derive PA $HP–OH^{\bullet}$ at O = 168 kcal/mol and PA $HP–OH^{\bullet}$ at P = 178 kcal/mol. These PA values are much higher than that of CO and thus a CO assisted tautomerization of $HP–OH_2^{\bullet+}$ is not expected to occur, in agreement with the experimental observations, which indicate that the ylide ion is exclusively generated.

Finally, we mention that the observed collision characteristics of the various isomeric ions are in complete agreement with the energy diagram presented in Scheme 7. If we compare the CID and MI mass spectra (Figs. 3 and 4) of for example **1a**, we see that loss of CO is insensitive towards collision. For a metastable fragmentation to be collision insensitive, the precursor ion must rearrange to a stable isomer via a transition state whose energy is higher than the dissociation threshold of the new isomer [17], exactly as is the case in Scheme 7.

3.3.2. *Oxygen equilibration reactions*

The above decarbonylation process becomes even more remarkable when the ^{18}O-labeling results are considered. The MI spectrum of **1a** ($^{18}OCH_3$) in Fig. 4 displays a 1:1 ratio for the loss of $C^{18}O$:$C^{16}O$ resulting in $H–P–^{16}OH_2^{\bullet+}$ and $H–P–^{18}OH_2^{\bullet+}$ of equal abundance. The same isotopic ratio is observed in the water loss products at *m/z* 60 and 62. On the other hand, there is a distinct, almost isotopically pure, loss of $P^{16}O^{\bullet}$ to form $CH_2{}^{18}OH^{+}$ at *m/z* 33. This indicates that the water loss and decarbonylation result from the same reacting ion, whereas the $PO^{\bullet}$ loss must occur from a different intermediate prior to oxygen equilibration. These results are supported by the ^{18}O-labeling experiments with **1b** ($P^{18}OH$). This ion also loses $C^{16}O$:$C^{18}O$ in a 1:1 ratio. The mirror effect for the $PO^{\bullet}$ loss is observed, in that now

$P^{18}O^{\bullet}$ is predominantly lost, again indicating that this fragmentation occurs from a different reacting ion configuration. Interestingly, the oxygen equilibration is only observed in the low-energy metastable ions **1b** ($P^{18}OH$); see Fig. 4, as opposed to the collisionally energized ions which do not show oxygen equilibration. *This indicates that the oxygen equilibration is a slow process with a fairly high energy requirement.*

Oxygen equilibration must involve a cyclic intermediate, which could be generated directly from either **1b** or **1d**, since these two ions have a methylene group available for bonding to an oxygen atom. Cyclization of **1d** would result in the symmetric ion **1e** (see Scheme 3) thus making the equilibration a simple ring closure—ring opening procedure. Ring opening of the original C–O bond results in ion **1d** with the oxygen atoms in reversed positions. However, as mentioned in Section 3.1, ion **1d** does not communicate with metastable ions **1a**/**b**. Furthermore, ion **1a**, which also displays the oxygen equilibration, communicates with **1b**, and not **1d**. This signifies that ion **1d** is not involved in the oxygen equilibration. Thus, it must be the cyclization of ion **1b** into ion **1f** which results in the oxygen atom equilibration. This is the rate-limiting step as the barrier to ring closure of ion **1b** lies 30 kcal/mol above ion **1b**. At this energy the ions (now in the **1f** configuration) can communicate easily with ID-**1c**, which in turn can easily isomerize into HBRC-**1c** below the threshold for dissociation into CH_2OH^+ and $PO^{\bullet}$ (see Scheme 8). Thus, the equilibration can be described as depicted in Scheme 5, viz. **1*b***(^{18}OH) → **1*f***(^{18}OH) → ID-**1*c***(^{18}OH) → HBRC-**1*c***($^{18}OCH_2$) → **1*b***($^{18}OCH_2$). This enables the oxygen atom equilibration to occur in the lower energy ions below the threshold for loss of $PO^{\bullet}$. No significant equilibration occurs for those ions that do lose $PO^{\bullet}$ as these higher energy metastable ions (ions **1b** with ca. 40 kcal/mol of internal energy) can communicate with HBRC-**1c** directly and will simply undergo the fast dissociation as opposed to passing through the slow equilibration process. Only the lower internal energy ions access the decarbonylation process with an internal energy content of 30–40 kcal/mol above **1b**.

Scheme 9 summarizes our results for the decarbonylation reactions starting from **1a**. Oxygen equilibration reactions are denoted as ↔, whereas the reactions that lead to decarbonylation follow the arrows →.

4. Conclusions

This study truly benefited from the synergy of theory and experiment. One without the other would not

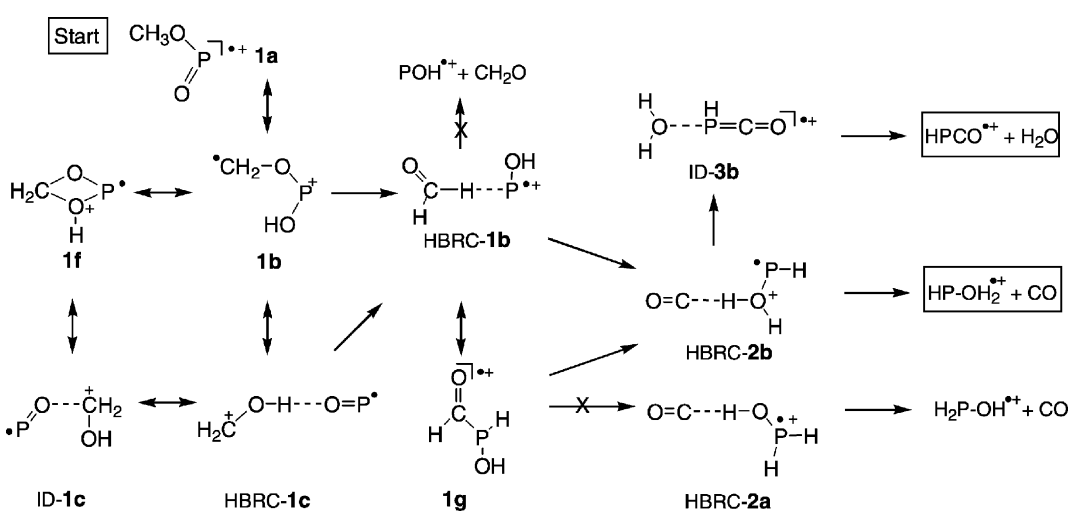

Scheme 9. Mechanism for decarbonylation (→) and for oxygen equilibration (↔) starting from **1a**.

have permitted to draw any solid mechanistic conclusion. That the oxygen atoms in metastable ions $CH_3O–P=O^{\bullet+}$ and $CH_2O–P–OH^{\bullet+}$ become equivalent in the decarbonylation and the accompanying H_2O loss was revealed by experiments on specifically labeled ions. Theory was used to differentiate between a priori plausible mechanisms for this equilibration. The CBS-QB3 calculations further revealed that metastable ions $CH_3O–P=O^{\bullet+}$ and $CH_2O–P–OH^{\bullet+}$ have a high propensity for rearrangement and that they can communicate with a great many stable isomers. The tandem mass spectrometry-based experiments established that the product ion generated in the decarbonylation is the ylide ion $HP–OH_2^{\bullet+}$, rather than $H_2P–OH^{\bullet+}$, which theory predicts to be the more stable isomer. The intricate details of the decarbonylation mechanism were revealed by theory, which indicates that $CH_2O–P–OH^{\bullet+}$ ions having a narrow range of internal energies at 36 kcal/mol, undergo a facile isomerization into the hydrogen-bridged ion $[HO–P\bullet\bullet\bullet H–C(H)=O]^{\bullet+}$, which further rearranges into another hydrogen-bridged radical cations, $[HP–O(H)–H\bullet\bullet\bullet C=O]^{\bullet+}$, the immediate precursor for decarbonylation into $HP–OH_2^{\bullet+}$.

Acknowledgements

J.K.T. thanks the Natural Sciences and Engineering Research Council of Canada (NSERC) for continuing financial support. L.N.H. thanks McMaster University for the Sherman Award and Micromass-Canada for its Graduate Student Award. P.J.A.R. thanks the Netherlands Organization for Scientific Research (NWO) for making available the SGI TERAS computer of SARA (Amsterdam). The contribution of Cathy Wong to the experimental work of this study is gratefully acknowledged.

References

[1] For selected recent references see: (a) A.J. Chalk, L. Radom, J. Am. Chem. Soc. 121 (1999) 1574;
(b) J. Chamot-Rooke, G. van der Rest, P. Mourgues, H.-E. Audier, Int. J. Mass Spectrom. 195/196 (2000) 385;
(c) M.A. Trikoupis, P.C. Burgers, P.J.A. Ruttink, J.K. Terlouw, Int. J. Mass Spectrom. 217 (2002) 97;
(d) M. Haranczyk, P.C. Burgers, P.J.A. Ruttink, Int. J. Mass Spectrom. 220 (2002) 53.
[2] L.N. Heydorn, Y. Ling, G. de Oliveira, J.M.L. Martin, Ch. Lifshitz, J.K. Terlouw, Zeitschrift für Physikalische Chemie 215 (2001) 141.
[3] (a) J.A. Montgomery Jr., M.J. Frisch, J.W. Ochterski, G.A. Petersson, J. Chem. Phys. 110 (1999) 2822;
(b) ibid. 112 (2000) 6532.
[4] L.N. Heydorn, P.C. Burgers, P.J.A. Ruttink, J.K. Terlouw, Int. J. Mass Spectrom. 227 (2003) 453.
[5] L.N. Heydorn, C.Y. Wong, R. Srinivas, J.K. Terlouw, Int. J. Mass Spectrom. 225 (2003) 11.
[6] L.N. Heydorn, P.C. Burgers, P.J.A. Ruttink, J.K. Terlouw, Chem. Phys. Lett. 368 (2003) 584.
[7] D.G. Hewitt, Aust. J. Chem. 32 (1979) 463.
[8] S.J. Fitch, J. Am. Chem. Soc. 86 (1964) 61.
[9] H.F. van Garderen, P.J.A. Ruttink, P.C. Burgers, G.A. McGibbon, J.K. Terlouw, Int. J. Mass Spectrom. Ion Proc. 121 (1992) 159.
[10] J.L. Holmes, J.K. Terlouw, Org. Mass Spectrom. 15 (1980) 383.
[11] M.J. Frisch, et al., Gaussian 98, Revision A.9, Gaussian, Inc., Pittsburgh, PA, 1998.
[12] (a) J.K. Terlouw, H. Schwarz, Angew. Chem. Int. Ed. Engl. 26 (1987) 805;
(b) M.A. Trikoupis, J.K. Terlouw, P.C. Burgers, M. Peres, C. Lifshitz, J. Am. Soc. Mass Spectrom. 10 (1999) 869.
[13] For selected recent review see: (a) G. Schalley, G. Hornung, D. Schröder, H. Schwarz, Chem. Soc. Rev. 27 (1998) 91;
(b) N. Goldberg, H. Schwarz, Acc. Chem. Res. 27 (1994) 34.
[14] J.L. Holmes, F.P. Lossing, J.K. Terlouw, P.C. Burgers, J. Am. Chem. Soc. 104 (1982) 2931.
[15] D.K. Böhme, Int. J. Mass Spectrom. Ion Proc. 115 (1992) 95.
[16] (a) E.P. Hunter, S.G. Lias, J. Phys. Chem. Ref. Data 27 (1998) 41;
(b) CBS-QB3 (298 K) values, this work.
[17] Y-P. Tu, J.L. Holmes, J. Am. Chem. Soc. 122 (2000) 3695.